



**RESEARCH ARTICLE**

# Scale interactions between the meso- and synoptic scales and the impact of diabatic heating

Mirjam Hirt<sup>1</sup>  | George C. Craig<sup>1</sup>  | Rupert Klein<sup>2</sup>

<sup>1</sup>Meteorological Institute,  
Ludwig-Maximilians-Universität,  
München, Germany

<sup>2</sup>Institute for Mathematics, Freie  
Universität Berlin, Berlin, Germany

**Correspondence**

Mirjam Hirt, Meteorological Institute,  
Ludwig-Maximilians-Universität, 80333  
München, Germany.  
Email: [m.hirt@lmu.de](mailto:m.hirt@lmu.de)

**Funding information**

German Research Foundation (DFG),  
Grant/Award Number: SFB / TRR 165  
“Waves to Weather”

**Abstract**

For both the meso- and synoptic scales, reduced mathematical models give insight into their dynamical behaviour. For the mesoscale, the weak temperature gradient approximation is one of several approaches, while for the synoptic scale the quasigeostrophic theory is well established. However, the way these two scales interact with each other is usually not included in such reduced models, thereby limiting our current perception of flow-dependent predictability and upscale error growth. Here, we address the scale interactions explicitly by developing a two-scale asymptotic model for the meso- and synoptic scales with two coupled sets of equations for the meso- and synoptic scales respectively. The mesoscale equations follow a weak temperature gradient balance and the synoptic-scale equations align with quasigeostrophic theory. Importantly, the equation sets are coupled via scale-interaction terms: eddy correlations of mesoscale variables impact the synoptic potential vorticity tendency and synoptic variables force the mesoscale vorticity (for instance due to tilting of synoptic-scale wind shear). Furthermore, different diabatic heating rates—representing the effect of precipitation—define different flow characteristics. With weak mesoscale heating relating to precipitation rates of  $\mathcal{O}(6 \text{ mm} \cdot \text{h}^{-1})$ , the mesoscale dynamics resembles two-dimensional incompressible vorticity dynamics and the upscale impact of the mesoscale on the synoptic scale is only of a dynamical nature. With a strong mesoscale heating relating to precipitation rates of  $\mathcal{O}(60 \text{ mm} \cdot \text{h}^{-1})$ , divergent motions and three-dimensional effects become relevant for the mesoscale dynamics and the upscale impact also includes thermodynamical effects.

**KEYWORDS**

asymptotics, atmospheric dynamics, mesoscale, multiscale scale interactions, quasigeostrophic, synoptic scale

## 1 | INTRODUCTION

Our Earth's atmosphere is a multiscale system. It is characterized by a wide range of processes on myriad spatial and temporal scales. Microphysical and turbulent processes leading to precipitation occur on spatial scales from millimetres to kilometres, mesoscale systems such as squall lines have spatial scales of tens or hundreds of kilometres, and synoptic systems such as baroclinic waves easily extend a thousand kilometers or more. Importantly, all these different processes at different scales can influence each other. As a consequence, small-scale disturbances can grow to large scales, presumably limiting our ability to predict the weather (Lorenz, 1969b; Craig *et al.*, 2021). Our current lack of understanding of multiscale interactions and their physical mechanisms further limits our understanding of error growth and predictability (Zhang *et al.*, 2007; Durran and Gingrich, 2014; Bierdel *et al.*, 2017; Selz *et al.*, 2022), providing the underlying motivation for the present investigation.

Lorenz (1969b) proposed an elegant theory for the development of perturbations across scales based on nonlinear interactions in a homogeneous turbulent flow. From this idealized model, he was able to obtain quantitative estimates of the influence of different scales of motion on each other, and to estimate the limits of predictability of a multiscale flow. However, the theory is based on strong assumptions that the statistics of the flow are homogeneous, isotropic, and stationary, which ignores the qualitatively different character of the flow on different scales.

On synoptic scales in midlatitudes, the atmosphere remains close to geostrophic and hydrostatic balance. Expanding the hydrostatic primitive equations in Rossby number gives geostrophic balance at leading order, and the quasigeostrophic (QG) equations at first order. QG theory is a well-accepted mathematical model, and underpins our understanding of weather phenomena including Rossby-wave dynamics or barotropic and baroclinic instability (Vallis, 2017). What QG theory does not provide is insight into the dynamics of the mesoscale and smaller scales, where errors grow initially.

At present, there is no theory for the mesoscales that is as well established as QG theory for synoptic scales. In the mesoscale, the constraint provided by the Earth's rotation is weaker, requiring different approximations and opening the possibility of other processes becoming dominant. A conceptually simple idea is to generalize the QG equations for weaker rotation by going to higher order in the Rossby-number expansion (Charney, 1955). This leads to a more accurate approximation—for example, for highly curved flows (Davis and Emanuel, 1991)—but is still not appropriate for phenomena like convective systems, where the influence of rotation may be negligible.

Another approach is semigeostrophic theory, which considers flows that are anisotropic, with only one component of the wind in geostrophic balance (Hoskins and Bretherton, 1972; Craig, 1993). Such models are well applicable to atmospheric fronts, but, like Charney's nonlinear balance theory, they do not cover the range of phenomena seen in the mesoscale. A third alternative is centered around latent heat release, particularly from convection, and uses a different physical constraint, namely a balance between the diabatic heat source and adiabatic cooling of ascending air (Sobel and Bretherton, 2000). In this so-called weak temperature gradient (WTG) approximation, the divergent wind component is determined to leading order by the vertical motion balancing the heat source. As with QG theory, the WTG approximation applies to slowly varying motions, where transient gravity waves do not play a role. It is widely used for the tropical atmosphere, where the effects of the Earth's rotation are small, and there is evidence that it is also applicable to the mesoscale in midlatitudes (Klein, 2010; Craig and Selz, 2018), although the approximation is not as accurate as geostrophic balance on the synoptic scale. However, even if the WTG approximation is accepted as a useful theory for mesoscale motions, their interactions with other scales, particularly the synoptic scale, remain an open question.

To obtain a theory for how different scales interact, we need to understand how the mathematical approximations that are appropriate for the different scales are related. The review of Klein (2010) shows how equations that are commonly applied to different scales in the atmosphere (including the QG and WTG approximations) can be obtained by different distinguished limits that arise when different characteristic scales of motion are assumed. The single-scale asymptotic derivations can be extended to a multiscale analysis, to yield a consistent set of equations for motions on different scales that include interaction terms describing the influence of other scales. A number of recent examples illustrate how this method can be applied to the atmosphere. Dolaptchiev and Klein (2013) applied this approach to obtain equations for both synoptic and planetary scales. Further applications of such multiscale approaches can be found for instance in Klein and Majda (2006); Achatz *et al.* (2010); Hittmeir and Klein (2018); Boljka and Shepherd (2018); Klein *et al.* (2022) for various scales. Saujani and Shepherd (2006) used a related approach to develop a more general version of the QG model that is potentially also applicable to mesoscales, but without making specific scale assumptions. Shaw and Shepherd (2009) combine hydrostatic planetary-scale flow with nonhydrostatic mesoscale flow representative of convection and gravity waves.

The aim of this article is to derive and interpret a multiscale equation set applicable for synoptic and mesoscale

motions, which can be used in the future to understand better the processes that influence our atmosphere's predictability. First, we aim for an appropriate distinguished limit that combines the QG approximation on the synoptic scale with the WTG approximation on the mesoscale. We focus in particular on the interactions between the scales, that is, on how the synoptic scale influences the mesoscale and vice versa, and on the impact of diabatic heating on the multiscale dynamics. Finally, we investigate how the multiscale asymptotic framework can be used to obtain a physical insight into atmospheric flows where scale interactions occur, by considering the impact of an idealized mesoscale heat source on a geostrophically balanced tropospheric jet, as an example of a physically relevant upscale interaction.

This article is structured as follows. In Section 2, we introduce the scale-consistent equations from Klein (2010), the two-scale ansatz that we use for the meso- and synoptic scales, and the basic steps for deriving the final, two-scale asymptotic equation sets. A detailed derivation of the equations is given in the Appendix. We present two different equations sets in Sections 3 and 4, depending on weaker or stronger diabatic heating in the mesoscale, respectively. An idealized example is considered in Section 5 to understand better the response to an idealized heat source and to obtain a first, data-driven perspective of the asymptotic approach and the resulting equations. Finally, we summarize and discuss our results and interpretations in Section 6.

## 2 | GOVERNING EQUATIONS AND MULTISCALE ASYMPTOTIC METHOD FOR MESO- AND SYNOPTIC SCALES

To derive the two-scale model for the synoptic and mesoscale regimes, we follow closely the approaches taken in Klein (2010) for several single-scale asymptotic regimes and Dolaptchiev and Klein (2013) for the multiscale approach. We further distinguish two regimes with different mesoscale diabatic heating strengths based on the characteristic heating rates of mesoscale phenomena. This distinction is made because the strength of the diabatic heating is found to affect the leading-order dynamics in a qualitative manner.

### 2.1 | Governing, nondimensionalized equations

First, we require a set of primitive equations that are nondimensionalized using a set of seven independent

characteristic scales. These characteristic scales can be combined to give three independent dimensionless parameters describing key characteristics of the flow. Following Klein (2010), these dimensionless parameters are then written in terms of a small parameter  $\epsilon$  to obtain a distinguished limit that is characteristic for the atmospheric scales of interest. Further characteristic scales can be derived from the independent ones. We refer the reader to Klein (2010) for further details and explanations.

Some key—-independent and derived—characteristic scales that are used for the nondimensionalization are the following.

- $u_{\text{ref}} \sim 12 \text{ m} \cdot \text{s}^{-1}$ : reference velocity (horizontal and vertical)
- $T_{\text{ref}} \sim 273 \text{ K}$ : reference temperature
- $\Delta\theta \sim 40 \text{ K}$ : for example, vertical potential temperature difference in the troposphere
- $h_{\text{sc}} \sim 11 \text{ km}$ : density scale height (used to nondimensionalize  $x$ ,  $y$ , and  $z$ )
- $t_{\text{ref}} \sim 15 \text{ min}$ : reference time-scale (used to nondimensionalize  $t$ )

Further characteristic scales and the formulation of the dimensionless parameters in terms of  $\epsilon$  are given in Klein (2010).

The resulting nondimensional equations for the horizontal and vertical momentum equations, the thermodynamic equation, and the continuity equation are then given as<sup>1</sup>:

$$(\partial_t + \mathbf{v}_h \cdot \nabla_h + w\partial_z)\mathbf{v}_h + \epsilon(2\boldsymbol{\Omega} \times \mathbf{v})_h + \frac{\theta}{\epsilon}\nabla_h\tilde{\pi} = Q_v, \quad (1)$$

$$\epsilon(\partial_t + \mathbf{v}_h \cdot \nabla_h + w\partial_z)w + \epsilon^2(2\boldsymbol{\Omega} \times \mathbf{v})_v - \frac{\tilde{\theta}}{1 + \epsilon\theta} + (1 + \epsilon\bar{\theta})\partial_z\tilde{\pi} + \epsilon^2\tilde{\theta}\partial_z\tilde{\pi} = \epsilon Q_w, \quad (2)$$

$$\epsilon(\partial_t + \mathbf{v}_h \cdot \nabla_h + w\partial_z)\tilde{\theta} + w\partial_z\bar{\theta} = \frac{1}{\epsilon}Q_\theta, \quad (3)$$

$$\epsilon^2\partial_t\tilde{\pi} + \epsilon^2\mathbf{v}_h \cdot \nabla_h\tilde{\pi} + \epsilon^2w\partial_z\tilde{\pi} + \gamma\bar{\pi} \left( \nabla_h \cdot \mathbf{v}_h + \frac{1}{p}\partial_z(\bar{p}w) \right) + \epsilon^2\gamma\Gamma\tilde{\pi}(\nabla_h \cdot \mathbf{v}_h + \partial_z w) = \frac{\gamma\pi}{\theta}Q_\theta. \quad (4)$$

<sup>1</sup>We use equations 9 in Klein (2010) with  $\alpha_x = \alpha_t = 0$  and  $\alpha_\pi = 2$ . In combination with the multiscale ansatz given below, these values for  $\alpha$  enable the same scaling for the synoptic and mesoscale regimes as considered in Klein (2010). For the continuity equation, we further introduce the pseudodensity  $\bar{p} = \bar{\pi}^{1/(\Gamma\gamma)}$ . The third term in Equation 2 deviates from Klein (2010) equation 9b (there,  $\tilde{\theta}/\theta$ ), but is consistent with his equation 5b. This has no further implications, as the differences occur only at higher orders of  $\epsilon$ , which we do not consider here.

TABLE 1 Scaling ansatz for meso- and synoptic-scale coordinates.

	Horiz. scale	$x$	$y$	Temp. scale	$t$	Vert. scale	$z$
Non-dimens.	$h_{sc} \sim 11$ km	$x$	$y$	$t_{ref} \sim 15$ min	$t$	$h_{sc} \sim 11$ km	$z$
Mesoscale	$L_{meso} \sim 150$ km	$x_m = \epsilon x$	$y_m = \epsilon y$	$T_{meso} \sim 3.5$ h	$t_m = \epsilon t$	$h_{sc} \sim 11$ km	$z$
Synoptic-scale	$L_{syn} \sim 1100$ km	$x_s = \epsilon^2 x$	$y_s = \epsilon^2 y$	$T_{syn} \sim 1$ d	$t_s = \epsilon^2 t$	$h_{sc} \sim 11$ km	$z$

Note: The nondimensional coordinates  $x, y$  were scaled with regard to  $h_{sc} \sim 11$  km and  $t$  with regard to  $t_{ref} \sim 15$  min. Indices “m” and “s” refer to the meso- and synoptic scale, respectively. For the vertical scale, we use the same characteristic scale used for the nondimensionalization ( $h_{sc} \sim 11$  km) for both meso- and synoptic scales. These scalings are in line with the scales given by Klein (2010) and are representative of the actual scales for meso and synoptic processes in the atmosphere. The notation used here leaves room also to incorporate the convective scale at  $\mathcal{O}(\epsilon^0)$ , which is planned for future work.

The variables and parameters are the horizontal wind  $\mathbf{v}_h$ , the vertical wind  $w$ , the potential temperature  $\theta = (1 + \epsilon \bar{\theta}(z) + \epsilon^2 \tilde{\theta})$ , the Exner pressure  $\pi = \bar{\pi}(z) + \epsilon^2 \Gamma \tilde{\pi}$ , the pseudodensity  $\bar{p}(z)$ , the planetary rotation vector  $\mathbf{\Omega} = \mathbf{k}(f_0 + \epsilon \beta y_s)$ , and  $\Gamma = (\gamma - 1)/\gamma$  with the dry isentropic exponent  $\gamma$ . Furthermore, we have the source and sink terms  $Q_{v_h}$ ,  $Q_w$ , and  $Q_\theta$  for the horizontal momentum, vertical momentum, and diabatic heating, respectively. We use subscript “h” to denote the horizontal ( $x, y$ ) components and subscript “v” for the vertical component. The partial derivatives  $\partial_z$  and  $\partial_t$  correspond to the vertical and temporal derivatives, respectively. Variables with an overline, e.g.  $\bar{\theta}$ , only depend on  $z$ , while their tilde counterparts, that is,  $\tilde{\theta}$  and  $\tilde{\pi}$ , contain variability in the  $x, y, t$  dimensions as well (see also Equations 7 and 8 below).

## 2.2 | Multiscale asymptotic ansatz and characteristic diabatic heating rates

Second, we use a scaling ansatz for the characteristic meso- and synoptic scales as summarized in Table 1 and the corresponding multiscale asymptotic expansions for the variables.

We expect the mesoscale diabatic heating source  $Q_\theta$  to play a crucial role, due to the expected WTG, regime and we thus distinguish between a weak diabatic heating regime (weakDH) and a strong diabatic heating regime (strongDH) with mesoscale heating magnitudes in the range of 4 K/3.5 h and 40 K/3.5 h, respectively. If the heating rates are dominated by latent heat release, they can be related to precipitation rates of 6 and 60 mm · h<sup>-1</sup> for weak and strong heating, respectively (Klein *et al.*, 2022). Under weak temperature gradient balance, the heating rates translate further into vertical velocities of 0.12 and  $\sim 1.2$  m · s<sup>-1</sup> for weak and strong heating, respectively. Strong heating rates could occur, for instance, in deep convective updrafts of mesoscale convective systems (Houze Jr., 2004), while the weak heating rate relates more to the stratiform areas of mesoscale convective systems

(Liu *et al.*, 2021) or latent heat release in warm conveyor belts (Joos and Wernli, 2012; Martínez-Alvarado *et al.*, 2014).

We use the following multiscale asymptotic expansions with regard to  $\epsilon$  for the relevant variables, where we abbreviate the dependences  $\{x_m, y_m, t_m\}$  as  $X_m$  and  $\{x_s, y_s, t_s\}$  as  $X_s$ :

$$\mathbf{v}_h = \mathbf{v}_{h,0}(X_m, X_s, z) + \epsilon \mathbf{v}_{h,1}(X_m, X_s, z) + \epsilon^2 \mathbf{v}_{h,2}(X_m, X_s, z) + \dots, \quad (5)$$

$$w = \epsilon \alpha_w w_1(X_m, X_s, z) + \epsilon^2 w_2(X_m, X_s, z) + \epsilon^3 w_3(X_m, X_s, z) + \dots, \quad (6)$$

$$\pi = \bar{\pi}(z) + \epsilon^2 \Gamma \underbrace{[\tilde{\pi}_0(X_s, z) + \epsilon \tilde{\pi}_1(X_m, X_s, z) + \dots]}_{=: \tilde{\pi}}, \quad (7)$$

$$\theta = 1 + \epsilon \bar{\theta}(z) + \epsilon^2 \underbrace{[\tilde{\theta}_0(X_s, z) + \epsilon \tilde{\theta}_1(X_m, X_s, z) + \dots]}_{=: \tilde{\theta}}, \quad (8)$$

$$Q_\theta = \epsilon^2 \alpha_w Q_{\theta,2}(X_m, X_s, z) + \epsilon^3 Q_{\theta,3}(X_m, X_s, z) + \dots, \quad (9)$$

$$Q_w = \epsilon^2 Q_{w,2}(X_m, X_s, z) + \epsilon^3 Q_{w,3}(X_m, X_s, z) + \dots, \quad (10)$$

$$\mathbf{Q}_{v_h} = \epsilon \mathbf{Q}_{v_h,1}(X_m, X_s, z) + \epsilon^2 \mathbf{Q}_{v_h,2}(X_m, X_s, z) + \dots. \quad (11)$$

In the ansatz for  $Q_\theta$ , we use  $\alpha_w = \{0, 1\}$  to distinguish between the weakDH ( $\alpha_w = 0$ ) and strongDH ( $\alpha_w = 1$ ) regimes. Due to the weak temperature approximation at leading orders for  $w$  (see Equation 28), this distinction affects the scaling of  $w$  accordingly (see  $\alpha_w$  in Equation 6). With  $\alpha_w = 1$ , these multiscale asymptotic expansions are in line with the two single-scale expansions given in Klein (2010) for his meso- $\beta^2$  and synoptic scales. Note that  $t_m$ , which represents the fastest time-scale accounted for in this expansion, corresponds to the advection time

<sup>2</sup>Our scaling corresponds to the weak-temperature-gradient scaling for the mesoscale with  $a = 1$  as given by Klein (2010).

at mesoscales. Thus, by the asymptotic ansatz, the faster internal waves, which are assumed to be in balance, are suppressed.

Following Dolaptchiev and Klein (2013) for the multiscale approach, we treat the meso- and synoptic-scale coordinates as if they were independent dimensions and use the following operators:

$$\nabla_h = \epsilon \nabla_m + \epsilon^2 \nabla_s, \quad (12)$$

$$\partial_t = \epsilon \partial_{t_m} + \epsilon^2 \partial_{t_s}. \quad (13)$$

A single vertical scale has been used for both meso- and synoptic-scale regimes, since motions on both horizontal scales can extend through the troposphere.

### 2.3 | Sublinear growth condition and averaging procedure

Next, we require a so-called sublinear-growth condition to obtain sufficiently robust expansions: all variables in the expansions, e.g.  $\mathbf{v}_{h,0}(X_m, X_s, z)$ , have to grow less than linearly in the mesoscale coordinates. A practical consequence of this condition is that any averages in the mesoscale coordinates vanish when applied to mesoscale derivatives:

$$\overline{\frac{\partial}{\partial X_m} v_i(X_m, X_s, \dots)} = 0, \quad (14)$$

where the averaging of a variable  $v_i(X_m, X_s, \dots)$  over a mesoscale averaging scale  $L_m$  is defined as

$$\overline{v_i(X_s, \dots)} = \lim_{\epsilon \rightarrow 0} \frac{\epsilon}{2L_m} \int_{\frac{X_s - L_m}{\epsilon}}^{\frac{X_s + L_m}{\epsilon}} v_i(X_m, X_s, \dots) dX_m. \quad (15)$$

Note that  $X_m = X_s/\epsilon$ . See Dolaptchiev and Klein (2013) for further details.

This averaging procedure allows us to decompose all our variables into a synoptic part, that is the average over the mesoscale, and a residual, describing the mesoscale fluctuating part:

$$v_i(X_m, X_s, \dots) = \overline{v_i(X_s, \dots)} + v_i^{\text{res}}(X_m, X_s, \dots) \\ = v_{i,s}(X_s, \dots) + v_{i,m}(X_m, X_s, \dots) \quad (16)$$

Given characteristic scales for synoptic-scale vertical velocities of  $\mathcal{O}(0.01 \text{ m} \cdot \text{s}^{-1})$  (Wallace and Hobbs, 2006), we assume  $\overline{w_1} = \overline{w_2} = 0$ . It follows that  $\overline{Q_{\theta,2}} = \overline{Q_{\theta,3}} = 0$  as well. We further set  $\overline{Q_{v,1}} = 0$ , which allows for geostrophic balance.

### 2.4 | Procedure for deriving the two-scale asymptotic model

Given these prerequisites, we can now derive a two-scale asymptotic model for the meso- and synoptic scales by executing the following steps.

- 1 Put the multiscale ansatz into all equations.
- 2 For each equation, collect terms with the same order of magnitude in  $\epsilon$ , as they need to balance each other.
- 3 Decompose fields into meso- and synoptic-scale parts.
- 4 Compute average and residual equations to obtain separate equations for the two scales. This reveals the *upscale/downscale* impact, where prognostic equations for synoptic/mesoscale variables may contain forcing terms involving mesoscale/synoptic variables, respectively.
- 5 Derive vorticity, QGPV, horizontal divergence equations.

The execution of these steps can be found in Appendix A.

## 3 | TWO-SCALE ASYMPTOTIC MODEL FOR THE WEAKDH REGIME ( $\alpha_w=0$ )

For the weakDH regime with a mesoscale diabatic heating scale of  $4 \text{ K}/3.5 \text{ h}$  (translating to a vertical velocity scale of  $0.12 \text{ m} \cdot \text{s}^{-1}$  or a precipitation rate of  $6 \text{ mm} \cdot \text{h}^{-1}$  via latent heating), we set  $\alpha_w = 0$  so that  $Q_{\theta,2}$  and  $w_1$  vanish in our expansions (see Equation A9). This simplifies the resulting asymptotic equations and we obtain a closed set of coupled equations for the synoptic and mesoscale variables as follows.

Indeed, at the mesoscale, the thermodynamic equation reduces to the following weak temperature gradient, as expected (see Equation A10):

$$w_2 \partial_z \overline{\theta} = Q_{\theta,3}. \quad (17)$$

The mesoscale dynamics are described further by a mesoscale vorticity equation with the relative mesoscale vorticity  $\zeta_m = \mathbf{k} \cdot \nabla_m \times \mathbf{v}_{0,m}$  and the two leading-order continuity equations (see Equations A30, A2, and A5, respectively):

$$\partial_{t_m} \zeta_m + \underbrace{\nabla_m \cdot (\zeta_m \mathbf{v}_{0,m})}_{\text{Mesoscale vorticity flux}} + \underbrace{\mathbf{v}_{0,s} \cdot \nabla_m \zeta_m}_{\text{synoptic advection of } \zeta_m} \\ = \mathbf{k} \cdot \nabla_m \times Q_{v,1}, \quad (18)$$

$$\nabla_m \cdot \mathbf{v}_{0,m} = 0, \quad (19)$$

$$\nabla_{\mathbf{m}} \cdot \mathbf{v}_{1,m} + \nabla_{\mathbf{s}} \cdot \mathbf{v}_{0,m} + \frac{1}{\bar{p}} \partial_z (\bar{p} w_2) = 0. \quad (20)$$

For the synoptic scale, we obtain a quasigeostrophic potential vorticity (QGPV) equation (see Equation A33):

$$\begin{aligned} & \underbrace{\partial_s q_s}_{\text{(I) syn. QGPV tendency}} + \underbrace{\nabla_s \cdot (\bar{v}_{0,s} q_s)}_{\text{(II) syn. QGPV advection}} \\ & + \underbrace{\partial_{x_s} \partial_{y_s} \overline{v_{0,m} v_{0,m}} - \partial_{x_s} \partial_{y_s} \overline{u_{0,m} u_{0,m}} + \partial_{x_s} \partial_{x_s} \overline{u_{0,m} v_{0,m}} - \partial_{y_s} \partial_{y_s} \overline{u_{0,m} v_{0,m}}}_{\text{(III-VI) Reynolds stress terms: } \mathbf{k} \cdot \nabla_s \times (\nabla_s^T \cdot (\mathbf{v}_{0,m} \mathbf{v}_{0,m}^T))^T} \\ & + \underbrace{\frac{1}{\bar{p}} \partial_z (\bar{p} \mathbf{k} \cdot \nabla_s \times \overline{\mathbf{v}_{0,m} w_2})}_{\text{(VII) vertical eddy flux}} \\ & = \underbrace{\mathbf{k} \cdot \nabla_s \times Q_{\mathbf{v},2,s} + \frac{f_0}{\bar{p}} \partial_z \left( \frac{\bar{p}}{\partial_z \theta} Q_{\theta_4} \right)}_{\text{source terms}}, \end{aligned} \quad (21)$$

with the synoptic-scale quasigeostrophic potential vorticity (PV)  $q_s$ :

$$q_s = \bar{k} \cdot \nabla_s \times \bar{v}_{0,s} + \beta y_s + \frac{f_0}{\bar{p}} \partial_z \left( \frac{\bar{p}}{\partial_z \theta} \bar{\theta}_0 \right). \quad (22)$$

In addition, we have the synoptic-scale thermodynamic equation, the first two continuity equations, and equations for geostrophic and hydrostatic balance, respectively (see Equations A14,A4,A7,A25, and A16):

$$\partial_t \bar{\theta}_0 + \mathbf{v}_{0,s} \cdot \nabla_s \bar{\theta}_0 + w_{3,s} \partial_z \bar{\theta} = \overline{Q_{\theta_4}}, \quad (23)$$

$$\nabla_s \cdot \bar{v}_{0,s} = 0, \quad (24)$$

$$\nabla_s \cdot \mathbf{v}_{1,s} + \frac{1}{\bar{p}} \partial_z (\bar{p} w_{3,s}) = 0, \quad (25)$$

$$\underbrace{f_0 \bar{k} \times \bar{v}_{0,s} + \nabla_s \bar{\pi}_0}_{\text{geostr. balance}} = 0, \quad (26)$$

$$\partial_z \bar{\pi}_0 = \bar{\theta}_0. \quad (27)$$

### 3.1 | Mesoscale dynamics

On the mesoscale, we obtain a weak temperature gradient balance so that diabatic heating is balanced by the vertical motion  $w_2$  (Equation 17). The leading-order horizontal wind is nondivergent (Equation 19), that is, the vertical

motion—generated by weak diabatic heating—is too weak to drive a horizontal divergence of the leading-order horizontal wind on the mesoscale. The vertical motion  $w_2$  does affect the mesoscale horizontal divergence of  $\mathbf{v}_{1,m}$  and the synoptic-scale horizontal divergence of  $\mathbf{v}_{0,m}$  in Equation 20. The latter will become relevant for the upscale-scale interactions in the synoptic-scale PV equation (terms III–VI in Equation 21). The leading-order vorticity dynamics in the mesoscale (Equation 18) closely resemble 2D vorticity dynamics for incompressible flow (Vallis, 2017). In the absence of momentum sources, mesoscale vorticity is only modified due to mesoscale and synoptic-scale advection; neither the planetary vorticity  $f_0$  nor the mesoscale diabatic heating/horizontal divergence contributes to mesoscale vorticity production. The advection of mesoscale vorticity by the synoptic wind is the only downscale influence from the synoptic to the mesoscale. From the mesoscale's perspective, this corresponds to vorticity advection via the large-scale background wind field.

### 3.2 | Synoptic-scale dynamics

On the synoptic scale, the dynamics follow QG theory closely, with additional mesoscale influences via eddy correlation terms. As we expect from regular QG theory, the leading-order synoptic wind is nondivergent (Equation 24) and follows geostrophic balance (Equation 26). When we neglect all mesoscale interaction terms in the PV equation (Equation 21), we obtain the PV equation given by regular QG theory, with a conservation of QGPV (terms I and II) in the absence of momentum sources and diabatic heating. The advantage of this multiscale model, however, is that the synoptic QGPV is now also influenced by mesoscale interaction terms, terms III–VII. Terms III–VI can be regarded as the synoptic-scale rotation of the horizontal divergence of a mesoscale horizontal Reynolds stress term acting in a diffusive manner. Note that these terms also include the synoptic-scale horizontal divergence of the mesoscale wind fields (see Equation A33), making the upscale impact from a mesoscale diabatic heat source more apparent. Term VII represents the impact of a vertical eddy momentum flux on the synoptic QGPV. Interestingly, these terms only represent a dynamical upscale influence on the QGPV without a thermodynamical upscale impact on the synoptic QGPV. Due to the eddy nature of these terms, the specific structure of the mesoscale flow field is critical to understanding the impact of these scale-interaction terms. The specific relevance and contributions of these terms for realistic atmospheric flow constellations will need to be identified in state-of-the-art weather simulations. To bridge the gap from mathematical asymptotic theory to such comprehensive simulations,

we study the multiscale response to diabatic heating in an idealized numerical framework in Section 5.

To summarize, the weakDH regime depicts a fairly passive role of mesoscale flow, which follows 2D vorticity dynamics for incompressible fluids, without further vorticity generation/destruction processes at leading order other than advection and momentum sources. The mesoscale diabatic heating is balanced by mesoscale vertical motion due to the WTG balance, but has no direct impact on  $\zeta_{0,m}$ . However, it projects upscale on the synoptic QGPV via the eddy flux terms.

#### 4 | TWO-SCALE ASYMPTOTIC MODEL FOR STRONGDH ( $\alpha_w=1$ )

We now consider the resulting asymptotic equations for flows with stronger diabatic heating, that is, with  $\alpha_w = 1$  and dimensional heating rates of 40 K/3.5 h (translating to a vertical velocity scale of  $1.2 \text{ m} \cdot \text{s}^{-1}$  or a precipitation rate of  $60 \text{ mm} \cdot \text{h}^{-1}$  via latent heating), as proposed in Klein (2010). Note that  $\alpha_w = 1$  is left in the equations to highlight the differences from the previous regime.

On the mesoscale, we now have the first- and second-order thermodynamic equations (see Equations A9,A10):

$$\alpha_w w_1 \partial_z \bar{\theta} = \alpha_w Q_{\theta,2}, \quad (28)$$

$$\alpha_w w_1 \partial_z \tilde{\theta}_0 + w_2 \partial_z \bar{\theta} = Q_{\theta,3}. \quad (29)$$

The vorticity equation (see Equation A30) reads

$$\begin{aligned} \partial_{t_m} \zeta_m + \underbrace{\nabla_m \cdot ((\zeta_m + f_0) \mathbf{v}_{0,m})}_{\text{(II) Mesoscale abs. vorticity flux}} + \underbrace{\alpha_w (\mathbf{k} \cdot \nabla_m w_1 \times \partial_z \mathbf{v}_{0,m})_{\text{res}}}_{\text{(III) mesoscale tilting}} \\ + \underbrace{\alpha_w (w_1 \partial_z \zeta_m)_{\text{res}}}_{\text{(IV) vert. advection of } \zeta_m} + \underbrace{\mathbf{v}_{0,s} \cdot \nabla_m \zeta_m}_{\text{(V) synoptic advection of } \zeta_m} \\ + \underbrace{\alpha_w \mathbf{k} \cdot \nabla_m w_1 \times \partial_z \mathbf{v}_{0,s}}_{\text{(VI) tilting of synoptic wind}} = \mathbf{k} \cdot \nabla_m \times Q_{v,1}. \end{aligned} \quad (30)$$

We also have the following continuity equations and hydrostatic balance in the mesoscale (see Equations A2,A5, and A19):

$$\nabla_m \cdot \mathbf{v}_{0,m} + \frac{\alpha_w}{p} \partial_z (\bar{p} w_1) = 0, \quad (31)$$

$$\nabla_m \cdot \mathbf{v}_{1,m} + \nabla_s \cdot \mathbf{v}_{0,m} + \frac{1}{p} \partial_z (\bar{p} w_2) = \alpha_w Q_{\theta,2}, \quad (32)$$

$$\partial_z \tilde{\pi}_{1,m} = \tilde{\theta}_{1,m}. \quad (33)$$

We can determine  $\tilde{\pi}_{1,m}$  with the mesoscale, horizontal divergence equation (see Equation A36):

$$\nabla_m^2 \tilde{\pi}_{1,m} = f(\mathbf{v}_{0,m}, \mathbf{v}_{0,s}, w_1, Q_{v,1}). \quad (34)$$

For the synoptic scale, we again obtain the following PV equation (see Equation A33):

$$\begin{aligned} \underbrace{\partial_{t_s} q_s}_{\text{(I) syn. PV tendency}} + \underbrace{\nabla_s \cdot (\tilde{\mathbf{v}}_{0,s} q_s)}_{\text{(II) syn. PV advection}} \\ + \underbrace{\partial_{x_s} \partial_{y_s} \overline{v_{0,m} v_{0,m}} - \partial_{x_s} \partial_{y_s} \overline{u_{0,m} u_{0,m}} + \partial_{x_s} \partial_{x_s} \overline{u_{0,m} v_{0,m}} - \partial_{y_s} \partial_{y_s} \overline{u_{0,m} v_{0,m}}}_{\text{(III-VI) Reynolds stress terms: } \mathbf{k} \cdot \nabla_s \times (\nabla_s^T \cdot \overline{\mathbf{v}_{0,m} \mathbf{v}_{0,m}^T})^T} \\ + \underbrace{\frac{1}{p} \partial_z (\bar{p} \mathbf{k} \cdot \nabla_s \times \overline{\mathbf{v}_{0,m} w_2}) + \frac{\alpha_w}{p} \partial_z (\bar{p} \mathbf{k} \cdot \nabla_s \times \overline{\mathbf{v}_{1,m} w_1})}_{\text{(VII, VIII) vertical eddy fluxes}} \\ + \underbrace{\frac{\alpha_w f_0}{p} \partial_z \left( \frac{1}{\partial_z \theta} \partial_z (\bar{p} w_1 \tilde{\theta}_{1,m}) \right)}_{\text{(IX) vert. eddy temperature flux}} \\ = \underbrace{\mathbf{k} \cdot \nabla_s \times Q_{v,2,s} + \frac{f_0}{p} \partial_z \left( \frac{\bar{p}}{\partial_z \theta} \overline{Q_{\theta,4}} \right)}_{\text{(X, XI) source terms}}. \end{aligned} \quad (35)$$

The synoptic-scale prognostic equation for  $\tilde{\theta}_0$  (thermodynamic equation) now takes the following form (see Equation A12):

$$\partial_{t_s} \tilde{\theta}_0 + \mathbf{v}_{0,s} \cdot \nabla_s \tilde{\theta}_0 + w_{3,s} \partial_z \bar{\theta} + \frac{\alpha_w}{p} \partial_z (\bar{p} w_1 \tilde{\theta}_{1,m}) = \overline{Q_{\theta,4}}. \quad (36)$$

Further diagnostic equations for the synoptic scale include averaged  $\mathcal{O}(\epsilon^2)$  and  $\mathcal{O}(\epsilon^3)$  continuity equations, the averaged  $\mathcal{O}(\epsilon^1)$  horizontal momentum equation, and the  $\mathcal{O}(\epsilon^0)$  vertical momentum equation (hydrostatic balance; see Equations A4,A7,A25, and A16):

$$\nabla_s \cdot \tilde{\mathbf{v}}_{0,s} = 0, \quad (37)$$

$$\nabla_s \cdot \mathbf{v}_{1,s} + \frac{1}{p} \partial_z (\bar{p} w_{3,s}) = 0, \quad (38)$$

$$\underbrace{f_0 \vec{k} \times \tilde{\mathbf{v}}_{0,s} + \nabla_s \tilde{\pi}_0}_{\text{geostr. balance}} + \frac{\alpha_w}{p} \partial_z (\bar{p} w_1 \tilde{\mathbf{v}}_{0,m}) = 0, \quad (39)$$

$$\partial_z \tilde{\pi}_0 = \tilde{\theta}_0. \quad (40)$$

To close the equations and obtain an explicit expression for the vertical eddy flux of  $\mathbf{v}_{1,m}$  in the synoptic PV equation (Equation 35, term VIII), a relatively involved analytical procedure designed to solve for  $\mathbf{v}_{1,m}$  and to guarantee its sublinear growth in both fast time and space variables is required. A similar task, although for the somewhat simpler problem of shallow-water flow over small-scale orography, was carried out by Bresch *et al.* (2011). A brief summary of the key ideas behind the procedure is provided in Appendix B, but we defer a more detailed study to a forthcoming work. Alternatively, one may use a more conventional closure, Stull (1988), or assume  $\overline{w_1 \mathbf{v}_{1,m}} = 0$  to eliminate the corresponding term for now. This has no major consequences for the other equations and all other terms remain, and we proceed along these lines in the rest of the article.

#### 4.1 | Mesoscale dynamics

With the stronger diabatic heating, the mesoscale dynamics changes comprehensively in comparison to the previous regime.

The weak temperature gradient balance now holds for  $w_1$ , which is determined by the leading-order diabatic heating  $Q_{\theta,2}$  (see Equation 28). The next order of the vertical velocity,  $w_2$ , can be determined by a modified WTG balance (Equation 29):  $w_2$  is balanced not only by the diabatic heating  $Q_{\theta,3}$ , but also by a scale interaction term manifesting as vertical temperature advection, where the synoptic-scale temperature variations  $\tilde{\theta}_0$  are advected with  $w_1$ .

The mesoscale temperature and pressure fields are in hydrostatic balance (Equation 33) and can be determined via the mesoscale horizontal divergence (Equation 34). The mesoscale temperature field  $\tilde{\theta}_{1,m}$  is then required to determine the eddy temperature flux in the synoptic PV equation.

In this strong heating regime, the leading-order mesoscale wind has a divergent component which is balanced by  $w_1$  (Equation 31). Its rotational component ( $\zeta_{0,m}$ , Equation 30) is generated and destroyed via several more processes in addition to the advection terms from the previous regime. The mesoscale flux term of absolute vorticity (term II) can be decomposed into  $\mathbf{v}_{0,m} \cdot \nabla_m (\zeta_m + f_0) + \zeta_m \nabla_m \cdot \mathbf{v}_{0,m} + f_0 \nabla_m \cdot \mathbf{v}_{0,m}$ , which includes the previous mesoscale advection term but also two stretching terms due to relative and planetary vorticity. The mesoscale tilting term (term III) corresponds to the transformation of horizontal vorticity due to vertical wind shear  $\partial_z \mathbf{v}_{0,m}$  into vertical vorticity  $\zeta_{0,m}$  via tilting by  $w_1$  gradients. The vertical advection term of  $\zeta_{0,m}$  (term IV) now also contributes to changes of  $\zeta_{0,m}$ , as the vertical velocity  $w_1$  is

now sufficiently strong to advect  $\zeta_{0,m}$  with a leading-order impact. The synoptic scale influences the mesoscale vorticity via the synoptic advection term (term V), as before, but also via a scale-interacting tilting term (term VI): the horizontal vorticity related to the vertical wind shear of the synoptic wind is tilted by  $w_1$  gradients and transformed to the mesoscale horizontal vorticity  $\zeta_{0,m}$ . Hence, in contrast to the weak-heating regime, we now observe a relatively direct impact of mesoscale diabatic heating on the mesoscale vorticity dynamics, manifesting in terms II, III, IV, VI via  $w_1$  or  $\nabla_m \cdot \mathbf{v}_{0,m}$  (see Equations 28,31).

The higher order continuity equation (Equation 32) is directly affected by the diabatic heating  $Q_{\theta,2}$  due to thermal expansion: the diabatic heating results in temperature-related density changes, thereby impacting the balance between the two horizontal divergence terms and the vertical gradient of  $w_2$ .

#### 4.2 | Synoptic-scale dynamics

While most aspects of the synoptic-scale dynamics are similar to the previous weak heating regime (nondivergent wind, hydrostatic balance, most scale interactions), two additional terms appear that provide further mesoscale influence on the synoptic scale. First, we have a vertical eddy temperature flux in the thermodynamic equation (Equation 36). Hence the mesoscale vertical velocity  $w_1$  is now strong enough to impact the synoptic  $\tilde{\theta}_0$  field via this eddy heat flux. As a consequence, the synoptic QGPV is now also modified by this thermodynamic process (term IX in Equation 35). Second, the geostrophic balance (Equation 39) is extended by an eddy momentum flux. Hence, with stronger diabatic heating, the leading-order synoptic wind does not follow the geostrophic wind any more, but is modified by mesoscale eddy momentum fluxes. (This resembles the eddy term in the antitriplic balance considered within the Ekman layer (see, e.g., (Markowski and Richardson, 2011)).

In summary, the stronger diabatic heating considered in this strongDH regime changes the leading-order mesoscale dynamics fundamentally by generating a leading-order divergent wind component and generating mesoscale vorticity via 3D effects. The synoptic scale is modified only by two additional interaction terms, modifying the geostrophic wind balance and providing a thermodynamic upscale impact on the synoptic QGPV.

### 5 | IDEALIZED EXAMPLE OF MULTISCALE WAVES

To obtain further physical insight into the multiscale framework, the equation sets obtained, and the multiscale



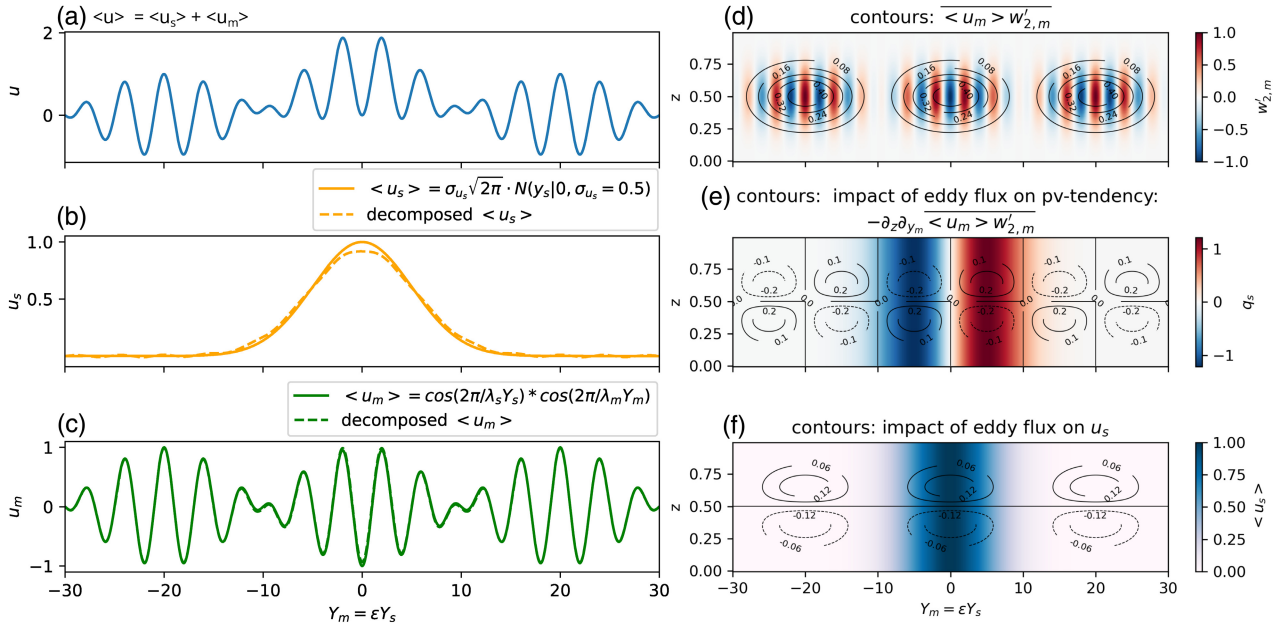


**FIGURE 1** Illustration of an idealized example with prescribed/imposed fields in color and the response/model outcome shown as contours. The meridional distribution for the prescribed, basic state zonal wind is shown in (a) for the total wind, (b) for the synoptic component  $\langle u_{0,s} \rangle$ , and (c) for the mesoscale component  $\langle u_{0,m} \rangle$ . (d) The meridional and vertical distribution of the imposed diabatic heating/vertical velocity (colors) and the eddy correlation  $\langle u_{0,m} \rangle w'_{2,m}$  from Equation 44 (contours). (e) The meridional and vertical distribution of the synoptic-scale QGPV (colors) and the impact from the eddy flux term (see Equation 44; contours). (f) The synoptic-scale zonal wind (colors) and how it is affected by the eddy flux (contours) [Colour figure can be viewed at [wileyonlinelibrary.com](http://wileyonlinelibrary.com)]

impact of diabatic heating, we consider an idealized example that resembles a midlatitude synoptic-scale barotropic jet stream with a mesoscale wave component in a slab-symmetric case<sup>3</sup> as displayed in Figure 1 (left column). We evaluate how a system with such prescribed wind fields responds linearly to an imposed mesoscale heat source of scale 4 K/3.5 h, that is, considering the weakDH regime. Other source/sink terms, for example, friction, are set to zero. Within the linear framework, we decompose our variables into a prescribed basic state denoted with  $\langle \rangle$  and a response denoted with a prime  $'$ : for example,  $u_0 = \langle u_0 \rangle + u'_0$ . Note that all variables are nondimensional as in our theoretical mode. We also treat the example from a numerical perspective, to bridge the gap between the mathematical asymptotic theory and its application in more realistic weather situations as given by numerical simulations. This will be helpful for future investigations, where state-of-the-art numerical weather simulations will be considered.

## 5.1 | Prescribed, basic state

We prescribe a basic state—denoted with  $\langle \rangle$ —of our idealized wind field that is stationary, nondivergent,

height-invariant, and without any vertical motion or meridional wind component:

$$\langle u_0 \rangle = \langle u_{0,m} \rangle(y_m, y_s) + \langle u_{0,s} \rangle(y_s), \quad (41)$$

$$\langle v_{0,m} \rangle = \langle v_{0,s} \rangle = \langle w_{2,m} \rangle = 0, \quad (42)$$

Specifically, we consider a synoptic-scale jetstream  $\langle u_{0,s} \rangle = \sigma_{u_s} \sqrt{2\pi} \cdot \mathcal{N}(y_s | 0, \sigma_{u_s})$ , which follows a Gaussian distribution with  $\sigma_{u_s} = 0.5$  in the meridional dimension as displayed in Figure 1b. Due to the height invariance of the jet stream, synoptic-scale potential temperature fluctuations are negligible, that is,  $\bar{\theta}_0 = 0$ . We superimpose this synoptic-scale component with a prescribed mesoscale wave, the amplitude of which varies on the synoptic scale, as shown in Figure 1c:  $\langle u_m \rangle = \cos[(2\pi/\lambda_s)y_s] \cdot \cos[(2\pi/\lambda_m)y_m]$  with  $\lambda_s = 4$  and  $\lambda_m = 4$ . The prescribed total zonal wind is illustrated in Figure 1a. In our numerical framework, we transform the  $y_s$  coordinate to our reference coordinate  $y_m$  via  $y_s = \epsilon y_m$  using  $\epsilon = 0.1$  and use a grid spacing of  $\Delta_{y_m} = 0.01$ . We approximate the averaging procedure (see Equation 15) using a Gaussian filter in the  $y$  dimension with  $\sigma_{y_m, \text{gaussianfilter}} = 2$ . Since the specific filter width is somewhat arbitrary,<sup>4</sup> we verify that the numerical

<sup>3</sup>All variables are constant in the zonal direction and vary only in the meridional or vertical direction.

<sup>4</sup>Following Equation 15, the effective filter size should be large with respect to the mesoscale coordinates, but small with respect to the synoptic-scale coordinate.

decomposition of the total zonal wind into synoptic and mesoscale components (see Equation 16) resembles our original synoptic and mesoscale structures (see dashed curves in Figure 1b,c, which are almost identical to the analytically computed ones). The same averaging procedure will then be used to compute the system's response.

Furthermore, we set  $\bar{p} = 1$  and  $\partial_z \bar{\theta} = 1$  for simplicity and set the Coriolis parameters  $f_0 = \beta = 0$ , as they do not contribute to the system's response in our idealized framework.

Derivatives are computed using finite differences with a finite-difference step of  $\Delta y_m = 0.01$ .

## 5.2 | Imposed diabatic heat source

Given this basic state, we now impose a diabatic heat source  $Q'_{\theta,3}(y_m, t_m, z) = w'_{2,m}$  (see Equation 17), which represents latent heat release from precipitating mesoscale clouds, and investigate the system's linear response. Specifically, we assume that the heat source follows the mesoscale jet stream  $\langle u_{0,m} \rangle$  in the meridional direction to maximize their eddy correlation, but with a Gaussian distribution in the vertical direction, see Figure 1d (colors):

$$Q'_{\theta,3} = \sigma_z \sqrt{2\pi} \mathcal{N}(z|0.5, \sigma_z = 0.15) \cdot \cos\left(\frac{2\pi}{\lambda_s} y_s\right) \cdot \cos\left(\frac{2\pi}{\lambda_m} y_m\right). \quad (43)$$

For simplicity, the heat source exists only during a short synoptic time interval  $\Delta t_s = 0.01$ , during which it remains constant.

We write the response of the system for any variable as its deviation from the stationary, height-invariant basic state, for example,  $u'_{0,m}(y_m, z, t_m) = u_{0,m}(y_m, z, t_m) - \langle u_{0,m} \rangle(y_m)$ . Any terms that are nonlinear in the prime ( $'$ ) variables are neglected due to the linearity assumption.

## 5.3 | Response to the heat source

The impact of the heat source on the mesoscale manifests in the vertical motion from the WTG balance. Otherwise, the diabatic heating source has no impact on the mesoscale vorticity dynamics.

There is, however, an upscale impact of the mesoscale heat source on the synoptic PV dynamics. Due to the design of our basic state and the linearity assumption, the PV equation (see Equation 21) reduces to

$$\partial_{t_s} q'_s = -\partial_{t_s} \partial_{y_s} u'_{0,s}$$

$$= -\underbrace{\partial_z (\partial_{y_s} \langle u_{0,m} \rangle w'_{2,m})}_{\text{(VII) vertical eddy flux}}. \quad (44)$$

The only remaining QGPV source is the vertical eddy flux term, which consists of the eddy correlation of the mesoscale zonal wind and the mesoscale vertical velocity/heat source. The vertical and meridional distribution of the eddy correlation is depicted in Figure 1d (contours), while its impact on the QGPV tendency is given in Figure 1e (contours), showing increases/reductions of QGPV gradients in the upper/lower troposphere. By considering its time evolution, the temporally integrated effect on the synoptic wind, that is,  $u'_{0,s}$  from Equation 44, is shown in Figure 1f (contours), where the jet stream is strengthened/weakened in the upper/lower troposphere.<sup>5</sup> We emphasize that the specific impact of the mesoscale heat source on the synoptic jet depends strongly on the eddy correlation of the mesoscale jet and the diabatic heat source.

To summarize, the imposed diabatic heat source is balanced by a vertical wind at the mesoscale, but does not affect mesoscale dynamics further. The heat source is projected upscale on the synoptic scale by a vertical eddy flux term, which modifies the synoptic jet stream, but it depends sensitively on how the mesoscale jet stream and the heat source are correlated. A more physical application of our multiscale equations using realistic numerical weather simulations is currently ongoing, where we hope to gain insight into realistic atmospheric conditions.

## 6 | SUMMARY AND DISCUSSION

In this work, we address how the meso- and synoptic scales interact with each other by following the approach from Klein (2010) and Dolaptchiev and Klein (2013). We developed a two-scale asymptotic model for the meso- and synoptic scales with two coupled sets of equations for the meso- and synoptic scales, respectively. The mesoscale equations follow a WTG balance and the synoptic-scale equations align with QG theory. Importantly, the equation sets are coupled via scale-interaction terms. Furthermore, we distinguish between weaker and stronger diabatic heating rates in the mesoscale—as proxy for the effect of latent heating. This distinction is made as it produces two

<sup>5</sup>The time evolution of the heat source does not have a qualitative impact on the system response. If the heat source lasts longer, for example, over a time period  $\Delta t_s = 1$ , the impact on the synoptic jet stream would simply be larger, but structurally identical.

qualitatively different regimes, the weakDH and strongDH regimes.

The weakDH regime is applicable to most mesoscale weather phenomena with moderate precipitation rates of  $\mathcal{O}(6 \text{ mm} \cdot \text{h}^{-1})$ , such as warm conveyor belts or stratiform precipitation from mesoscale convective systems. The mesoscale diabatic heating is balanced by adiabatic cooling from vertical motion following WTG balance. In contrast to traditional WTG theory, however, it has no direct impact on the leading-order mesoscale horizontal wind, which is nondivergent. Only at the next order does the corresponding WTG-related divergent motion occur. Consequently, the leading-order mesoscale vorticity closely follows 2D vorticity dynamics for incompressible flow, which is only modified by advection and momentum sources and is decoupled from the WTG-related vertical motion. There is a downscale influence from the synoptic scale via mesoscale vorticity advection with the synoptic-scale wind. The synoptic-scale dynamics is in geostrophic balance at leading order. The next-order synoptic-scale dynamics follows QG dynamics except for five eddy correlation terms in the PV equation, which describe a dynamical mesoscale impact on synoptic-scale QGPV generation. These terms can be interpreted as the impact of horizontal Reynolds stress and vertical eddy momentum flux on the vorticity dynamics.

The strongDH regime is applicable only for highly convective phenomena with very strong precipitation rates of  $\mathcal{O}(60 \text{ mm} \cdot \text{h}^{-1})$ , for example, deep convective areas within mesoscale convective systems. The leading-order vertical wind balances a stronger heat source and is now sufficiently strong to impact the leading-order mesoscale divergent wind similarly to traditional WTG theory. The mesoscale vorticity is additionally affected by planetary and relative vorticity stretching, tilting of horizontal vorticity, and vertical vorticity advection, that is, three-dimensional effects become relevant. In addition to the synoptic-scale advection term already relevant in the weakDH regime, another downscale interaction term becomes relevant, namely the tilting of horizontal vorticity from synoptic-scale wind shear. On the synoptic scale, the geostrophic balance is broken by an upscale eddy momentum flux term and the QGPV is further influenced by a thermodynamic upscale process related to eddy vertical temperature fluxes.

The distinction between weak and strong heating emphasizes the flow-dependent nature of the mesoscale. In the weakDH regime, the flow is dominated by 2D vorticity dynamics with negligible divergence and forced by the downscale vorticity advection. Such flow characteristics may relate to a downscale enstrophy cascade and a  $-3$  slope in the energy spectrum (Vallis, 2017). Similarly, Selz *et al.* (2019) have reported the mesoscale dynamics for dry

weather situations to be mostly nondivergent with a  $-3$  slope in the kinetic energy spectrum, and driven primarily by large-scale QGPV dynamics. In the strongDH regime, 3D effects and divergent motion become relevant for the mesoscale dynamics, which fits well with the observations from Selz *et al.* (2019) for precipitating weather situations, where divergent motions and a shallower kinetic energy spectrum are found.

An important application for this framework will be to derive error equations, that is, equations that describe the evolution of the difference between simulations starting from perturbed initial conditions, in order to provide further insight into our atmosphere's predictability. For instance, do the nonlinear triad interaction processes of Lorenz (1969a) dominate error growth in the weakDH regime, while upscale error growth is more relevant if the latent heat release is unusually strong and the strongDH equations apply? What processes can we identify to be most relevant for upscale error growth? Does that align with previous results from Bierdel *et al.* (2017); Baumgart *et al.* (2019), where divergent motion and geostrophic adjustment were identified as key contributors for how convective processes project errors upscale? We hope to gain further insight in the future.

Furthermore, we applied the multiscale asymptotic framework to an idealized numerical example, where a synoptic-scale zonal jet stream is superimposed on a weak mesoscale diabatic heating wave. Here, the vertical eddy momentum flux projects the mesoscale heat source on the synoptic scale, strengthening the upper tropospheric synoptic jet stream. However, because an eddy correlation between mesoscale vertical and horizontal motion is required, the impact on the synoptic jet stream is very sensitive to the specific mesoscale situation. Hence, more realistic situations need to be considered to make meaningful conclusions on the upscale behaviour of mesoscale diabatic heat sources. We are currently applying the mathematical asymptotic framework to numerical model output finite-scale separations, to investigate the validity of the approximations and the insight that can be obtained about the physical processes on different scales. This work will be reported in a forthcoming publication.

To conclude, by developing a two-scale asymptotic model, we have identified scale-interaction terms between the meso- and synoptic scales and found the strength of the mesoscale diabatic heating to determine key mesoscale flow properties such as divergence and 3D vorticity effects. The multiscale equations can now be used as a diagnostic tool for realistic weather simulations to gain deeper insights into the scale interactions, corresponding error-growth processes, and predictability limits of our atmosphere's many scales.

## AUTHOR CONTRIBUTIONS

**Mirjam Hirt:** conceptualization; formal analysis; methodology; visualization; writing – original draft; writing – review and editing. **George C. Craig:** conceptualization; formal analysis; funding acquisition; methodology; supervision; writing – review and editing. **Rupert Klein:** formal analysis; methodology; validation; writing – review and editing.

## ACKNOWLEDGEMENTS

The research leading to these results has been carried out within subproject A1 of the Transregional Collaborative Research Center SFB/TRR 165 “Waves to Weather” (<https://www.wavestoweather.de>) funded by the German Research Foundation (DFG). Rupert Klein appreciates support for his contributions by DFG Collaborative Research Centre CRC 1114 “Scaling Cascades in Complex Systems”, Project Number 235221301, Project C06 “Multiscale structure of atmospheric vortices”. Open Access funding enabled and organized by Projekt DEAL.

## ORCID

Mirjam Hirt  <https://orcid.org/0000-0002-5650-7594>

George C. Craig  <https://orcid.org/0000-0002-7431-8164>

## REFERENCES

- Achatz, U., Klein, R. and Senf, F. (2010) Gravity waves, scale asymptotics and the pseudo-incompressible equations. *Journal of Fluid Mechanics*, 663, 120–147.
- Baumgart, M., Ghinassi, P., Wirth, V., Selz, T., Craig, G.C. and Riemer, M. (2019) Quantitative view on the processes governing the upscale error growth up to the planetary scale using a stochastic convection scheme. *Monthly Weather Review*, 147, 1713–1731 URL <https://journals.ametsoc.org/view/journals/mwre/147/5/mwr-d-1%8-0292.1.xml>.
- Bierdel, L., Selz, T. and Craig, G. (2017) Theoretical aspects of upscale error growth through the mesoscales: an analytical model. *Quarterly Journal of the Royal Meteorological Society*, 143, 3048–3059 URL <https://rmets.onlinelibrary.wiley.com/doi/abs/10.1002/qj.3160>.
- Boljka, L. and Shepherd, T.G. (2018) A multiscale asymptotic theory of extratropical wave, mean-flow interaction. *Journal of the Atmospheric Sciences*, 75, JAS-D-17-0307.1 URL <http://journals.ametsoc.org/doi/10.1175/JAS-D-17-0307.1>.
- Bresch, D., Klein, R. and Lucas, C. (2011) Multiscale analyses for the shallow water equations. In: Krause, E., Shokin, Y., Resch, M., Kröner, D. and Shokina, N. (Eds.) *Computational Science and High Performance Computing IV*. Vol. 115 of Notes on Numerical Fluid Mechanics and Multidisciplinary Design, Berlin: Springer; pp. 149–163. [https://doi.org/10.1007/978-3-642-17770-5\\_12](https://doi.org/10.1007/978-3-642-17770-5_12)
- Charney, J. (1955) The use of the primitive equations of motion in numerical prediction. *Tellus*, 7, 22–26 URL <https://onlinelibrary.wiley.com/doi/abs/10.1111/j.2153-3490.1%955.tb01138.x>.
- Craig, G.C. (1993) A scaling for the three-dimensional semi-geostrophic approximation. *Journal of Atmospheric Sciences*, 50, 3350–3355 URL [https://journals.ametsoc.org/view/journals/atsc/50/19/1520-04%69\\_1993\\_050\\_3350\\_asfttd\\_2\\_0\\_co\\_2.xml](https://journals.ametsoc.org/view/journals/atsc/50/19/1520-04%69_1993_050_3350_asfttd_2_0_co_2.xml).
- Craig, G.C., Fink, A.H., Hoose, C., Janjić, T., Knippertz, P., Laurian, A., Lerch, S., Mayer, B., Miltenberger, A., Redl, R., Riemer, M., Tempest, K.I. and Wirth, V. (2021) Waves to weather: exploring the limits of predictability of weather. *Bulletin of the American Meteorological Society*, 102, E2151–E2164 URL <https://journals.ametsoc.org/view/journals/bams/102/11/BAMS-D%-20-0035.1.xml>.
- Craig, G.C. and Selz, T. (2018) Mesoscale dynamical regimes in the Midlatitudes. *Geophysical Research Letters*, 45, 410–417.
- Davis, C.A. and Emanuel, K.A. (1991) Potential vorticity diagnostics of cyclogenesis. *Monthly Weather Review*, 119, 1929–1953 URL [https://journals.ametsoc.org/view/journals/mwre/119/8/1520-04%93\\_1991\\_119\\_1929\\_pvdod\\_2\\_0\\_co\\_2.xml](https://journals.ametsoc.org/view/journals/mwre/119/8/1520-04%93_1991_119_1929_pvdod_2_0_co_2.xml).
- Dolaptchiev, S.I. and Klein, R. (2013) A multiscale model for the planetary and synoptic motions in the atmosphere. *Journal of the Atmospheric Sciences*, 70, 2963–2981 URL <https://doi.org/10.1175/JAS-D-12-0272.1>.
- Durran, D.R. and Gingrich, M. (2014) Atmospheric predictability: why butterflies are not of practical importance. *Journal of the Atmospheric Sciences*, 71, 2476–2488 URL <https://journals.ametsoc.org/view/journals/atsc/71/7/jas-d-14%0007.1.xml>.
- Hittmeir, S. and Klein, R. (2018) Asymptotics for moist deep convection I: refined scalings and self-sustaining updrafts. *Theoretical and Computational Fluid Dynamics*, 32, 137–164.
- Hoskins, B.J. and Bretherton, F.P. (1972) Atmospheric frontogenesis models: mathematical formulation and solution. *Journal of Atmospheric Sciences*, 29, 11–37 URL [https://journals.ametsoc.org/view/journals/atsc/29/1/1520-046%9\\_1972\\_029\\_0011\\_afmfa\\_2\\_0\\_co\\_2.xml](https://journals.ametsoc.org/view/journals/atsc/29/1/1520-046%9_1972_029_0011_afmfa_2_0_co_2.xml).
- Houze, R.A., Jr. (2004) Mesoscale convective systems. *Reviews of Geophysics*, 42, 5 URL <https://agupubs.onlinelibrary.wiley.com/doi/abs/10.1029/2004R%G000150>.
- Joos, H. and Wernli, H. (2012) Influence of microphysical processes on the potential vorticity development in a warm conveyor belt: a case-study with the limited-area model cosmo. *Quarterly Journal of the Royal Meteorological Society*, 138, 407–418 URL <https://rmets-onlinelibrary-wiley-com.emedien.ub.uni-muenchen.de/doi/abs/10.1002/qj.934>.
- Klein, R. (2010) Scale-dependent models for atmospheric flows. *Annual Review of Fluid Mechanics*, 42, 249–274 URL <https://doi.org/10.1146/annurev-fluid-121108-145537>.
- Klein, R. and Majda, A.J. (2006) Systematic multiscale models for deep convection on mesoscales. *Theoretical and Computational Fluid Dynamics*, 20, 525–551.
- Klein, R., Schielicke, L., Pfahl, S. and Khouider, B. (2022) Qg–dl–ekman: dynamics of a diabatic layer in the quasi-geostrophic framework. *Journal of the Atmospheric Sciences*, 79, 887–905 URL <https://journals.ametsoc.org/view/journals/atsc/79/3/JAS-D-21%0110.1.xml>.
- Liu, N., Leung, L.R. and Feng, Z. (2021) Global mesoscale convective system latent heating characteristics from gpm retrievals and an mcs tracking dataset. *Journal of Climate*, 34, 8599–8613 URL <https://journals.ametsoc.org/view/journals/clim/34/21/JCLI-D-%20-0997.1.xml>.
- Lorenz, E.N. (1969a) Atmospheric predictability as revealed by naturally occurring analogues. *Journal of the Atmospheric Sciences*, 26, 636–646 URL <http://journals.ametsoc.org/doi/abs/10.1175/1520-0469%2819%69%2926%3C636%3AAPARBN%3E2.0.CO%3B2>.

- Lorenz, E.N. (1969b) The predictability of a flow which possesses many scales of motion. *Tellus*, 21, 289–307 URL <http://tellusa.net/index.php/tellusa/article/view/10086>.
- Markowski, P. and Richardson, Y. (2011) *Mesoscale Meteorology in Midlatitudes*, Vol. 2. John Wiley & Sons. <https://doi.org/10.1002/9780470682104>
- Martínez-Alvarado, O., Joos, H., Chagnon, J., Boettcher, M., Gray, S.L., Plant, R.S., Methven, J. and Wernli, H. (2014) The dichotomous structure of the warm conveyor belt. *Quarterly Journal of the Royal Meteorological Society*, 140, 1809–1824 URL <https://rmets-onlinelibrary-wiley-com.emedien.uni-muenchen.de/doi/abs/10.1002/qj.2276>.
- Saujani, S. and Shepherd, T.G. (2006) A unified theory of balance in the extratropics. *Journal of Fluid Mechanics*, 569, 447–464.
- Selz, T., Bierdel, L. and Craig, G.C. (2019) Estimation of the variability of mesoscale energy spectra with three years of COSMO-DE analyses. *Journal of the Atmospheric Sciences*, 76, 627–637.
- Selz, T., Riemer, M. and Craig, G. (2022) The transition from practical to intrinsic predictability of midlatitude weather. *Journal of the Atmospheric Sciences*. URL <https://journals.ametsoc.org/view/journals/atsc/aop/JAS-D-21-0271.1/JAS-D-21-0271.1.xml>, 79, 2013–2030.
- Shaw, T.A. and Shepherd, T.G. (2009) A theoretical framework for energy and momentum consistency in subgrid-scale parameterization for climate models. *Journal of the Atmospheric Sciences*, 66, 3095–3114 URL <https://journals.ametsoc.org/jas/article/66/10/3095/26959/A-T%theoretical-Framework-for-Energy-and-Momentum>.
- Sobel, A.H. and Bretherton, C.S. (2000) Modeling tropical precipitation in a single column. *Journal of Climate*, 13, 4378–4392 URL [https://journals.ametsoc.org/view/journals/clim/13/24/1520-04%42\\_2000\\_013\\_4378\\_mtpias\\_2.0.co\\_2.xml](https://journals.ametsoc.org/view/journals/clim/13/24/1520-04%42_2000_013_4378_mtpias_2.0.co_2.xml).
- Stull, R.B. (1988) *An introduction to boundary layer meteorology*, Vol. 13. Dordrecht: Springer Science & Business Media. <https://link.springer.com/book/10.1007/978-94-009-3027-8>
- Vallis, G.K. (2017) *Atmospheric and oceanic fluid dynamics*. Cambridge: Cambridge University Press. <https://doi.org/10.1017/9781107588417>
- Wallace, J.M. and Hobbs, P.V. (2006) *Atmospheric science: an introductory survey*, Vol. 92. San Diego: Elsevier.
- Zhang, F., Bei, N., Rotunno, R., Snyder, C. and Epifanio, C.C. (2007) Mesoscale Predictability of Moist Baroclinic Waves: Convection-Permitting Experiments and Multistage Error Growth Dynamics. URL <https://journals.ametsoc.org/doi/pdf/10.1175/JAS4028.1>.

**How to cite this article:** Hirt, M., Craig, G.C. & Klein, R. (2023) Scale interactions between the meso- and synoptic scales and the impact of diabatic heating. *Quarterly Journal of the Royal Meteorological Society*, 149(753), 1319–1334. Available from: <https://doi.org/10.1002/qj.4456>

## APPENDIX A. FULL DERIVATION OF THE MULTISCALE MODEL

### A.1 Continuity equation

To derive the multiscale version of the continuity equation, we start with Equation 4, consider the ansatz given in Section 2.2, and follow the first step described in Section 2.4:

$$\begin{aligned}
 & \epsilon^3 \partial_{t_m} \tilde{\pi} + \epsilon^4 \partial_{t_s} \tilde{\pi} + \epsilon^3 \mathbf{v}_h \cdot \nabla_m \tilde{\pi} + \epsilon^4 \mathbf{v}_h \cdot \nabla_s \tilde{\pi} \\
 & + \epsilon^3 (\alpha_w w_1 + \epsilon w_2 + \dots) \partial_z \tilde{\pi} \\
 & + \gamma \bar{\pi} (\epsilon \nabla_m \cdot \mathbf{v}_h + \epsilon^2 \nabla_s \cdot \mathbf{v}_h \\
 & + \frac{\epsilon}{p} \partial_z [\bar{p} (\alpha_w w_1 + \epsilon w_2 + \dots)]) \\
 & + \epsilon^2 \gamma \Gamma \tilde{\pi} [\epsilon \nabla_m \cdot \mathbf{v}_h + \epsilon^2 \nabla_s \cdot \mathbf{v}_h \\
 & + \epsilon \partial_z (\alpha_w w_1 + \epsilon w_2 + \dots)] \\
 & = \frac{\gamma (\bar{\pi} + \epsilon^2 \tilde{\pi})}{1 + \epsilon \bar{\theta} + \epsilon^2 \tilde{\theta}} (\epsilon^2 \alpha_w Q_{\theta,2} + \epsilon^3 Q_{\theta,3} + \dots). \quad (A1)
 \end{aligned}$$

We use the Taylor series for  $\frac{1}{1 + \epsilon \bar{\theta} + \epsilon^2 \tilde{\theta}_0 + \dots} \approx 1 - \epsilon \bar{\theta} + \epsilon^2 (\bar{\theta}^2 - \tilde{\theta}_0) + \dots$ . Following steps 2–4 from Section 2.4, we separate the equation into different orders of  $\epsilon$ , average each resulting equation over the synoptic scale, and compute residual equations as the difference between the corresponding equation and its averaged version. We obtain the following equations for the first three orders of  $\epsilon$ :

$$\mathcal{O}(\epsilon^1) : \nabla_m \cdot \mathbf{v}_{0,m} + \frac{\alpha_w}{p} \partial_z (\bar{p} w_1) = 0, \quad (A2)$$

$$\mathcal{O}(\epsilon^2) : \nabla_m \cdot \mathbf{v}_{h,1} + \nabla_s \cdot \mathbf{v}_{h,0} + \frac{1}{p} \partial_z (\bar{p} w_2) = \alpha_w Q_{\theta,2}, \quad (A3)$$

$$\overline{\mathcal{O}(\epsilon^2)} : \nabla_s \cdot \mathbf{v}_{0,s} = 0, \quad (A4)$$

$$\mathcal{O}(\epsilon^2)_{\text{res}} : \nabla_m \cdot \mathbf{v}_{1,m} + \nabla_s \cdot \mathbf{v}_{0,m} + \frac{1}{p} \partial_z (\bar{p} w_2) = \alpha_w Q_{\theta,2}, \quad (A5)$$

$$\begin{aligned}
 \mathcal{O}(\epsilon^3) : & \frac{\alpha_w}{\gamma \bar{\pi}} w_1 \partial_z \tilde{\pi}_0 + \nabla_m \cdot \mathbf{v}_{h,2} + \nabla_s \cdot \mathbf{v}_{h,1} + \frac{1}{p} \partial_z (\bar{p} w_3) \\
 & + \frac{\tilde{\pi}_0 \Gamma}{\bar{\pi}} (\nabla_m \cdot \mathbf{v}_{h,0} + \alpha_w \partial_z w_1) = Q_{\theta,3} - \alpha_w \bar{\theta} Q_{\theta,2}, \quad (A6)
 \end{aligned}$$

$$\overline{\mathcal{O}(\epsilon^3)} : \nabla_s \cdot \mathbf{v}_{1,s} + \frac{1}{p} \partial_z (\bar{p} w_{3,s}) = 0. \quad (A7)$$

## A.2 Thermodynamic equation

$$\begin{aligned} & [e^2 \partial_{t_m} + e^3 \partial_{t_s} + e^2 \mathbf{v}_h \cdot \nabla_m + e^3 \mathbf{v}_h \cdot \nabla_s \\ & + e^2 (w_1 + \dots) \partial_z] (\bar{\theta}_0 + e\bar{\theta}_1 + \dots) \\ & + \epsilon (\alpha_w w_1 + \epsilon w_2 + \dots) \partial_z \bar{\theta} = \frac{1}{\epsilon} Q_\theta. \end{aligned} \quad (\text{A8})$$

We separate the equation into different orders of epsilon and average over the synoptic scale:

$$\mathcal{O}(\epsilon^1) : \alpha_w w_1 \partial_z \bar{\theta} = \alpha_w Q_{\theta,2}, \quad (\text{A9})$$

$$\mathcal{O}(\epsilon^2) : \alpha_w w_1 \partial_z \bar{\theta}_0 + w_2 \partial_z \bar{\theta} = Q_{\theta,3}, \quad (\text{A10})$$

$$\begin{aligned} \mathcal{O}(\epsilon^3) : & \partial_{t_m} \bar{\theta}_1 + \partial_{t_s} \bar{\theta}_0 + \mathbf{v}_{h,0} \cdot \nabla_m \bar{\theta}_1 \\ & + \mathbf{v}_{h,0} \cdot \nabla_s \bar{\theta}_0 + \alpha_w w_1 \partial_z \bar{\theta}_1 + w_2 \partial_z \bar{\theta}_0 \\ & + w_3 \partial_z \bar{\theta} = Q_{\theta,4}, \end{aligned} \quad (\text{A11})$$

$$\begin{aligned} \overline{\mathcal{O}(\epsilon^3)} : & \partial_{t_s} \bar{\theta}_0 + \overline{\mathbf{v}_{0,m} \cdot \nabla_m \bar{\theta}_{1,m}} \\ & + \mathbf{v}_{0,s} \cdot \nabla_s \bar{\theta}_0 + \overline{\alpha_w w_1 \partial_z \bar{\theta}_{1,m}} \\ & + w_{3,s} \partial_z \bar{\theta} = \overline{Q_{\theta,4}}. \end{aligned} \quad (\text{A12})$$

Using the continuity equation (Equation A5), we can formulate the mesoscale  $\bar{\theta}_{1,m}$  horizontal and vertical advection terms as vertical flux only:

$$\begin{aligned} & \partial_{t_s} \bar{\theta}_0 + \mathbf{v}_{0,s} \cdot \nabla_s \bar{\theta}_0 + w_{3,s} \partial_z \bar{\theta} \\ & + \underbrace{\overline{\mathbf{v}_{0,m} \cdot (\mathbf{v}_{0,m} \bar{\theta}_{1,m})}}_{=0} - \underbrace{\overline{\bar{\theta}_{1,m} \nabla_m \cdot \mathbf{v}_{0,m}}}_{-\frac{\alpha_w}{\bar{p}} \bar{\theta}_{1,m} \partial_z (\bar{p} w_1)} \\ & + \overline{\alpha_w w_1 \partial_z \bar{\theta}_{1,m}} = \overline{Q_{\theta,4}}. \end{aligned} \quad (\text{A13})$$

Then we obtain for the synoptic-scale thermodynamic equation

$$\begin{aligned} & \partial_{t_s} \bar{\theta}_0 + \mathbf{v}_{0,s} \cdot \nabla_s \bar{\theta}_0 + w_{3,s} \partial_z \bar{\theta} \\ & + \frac{\alpha_w}{\bar{p}} \partial_z (\overline{\bar{p} w_1 \bar{\theta}_{1,m}}) = \overline{Q_{\theta,4}}. \end{aligned} \quad (\text{A14})$$

## A.3 Vertical momentum equation

$$\begin{aligned} & [e^3 \partial_{t_m} + e^4 \partial_{t_s} + e^3 \mathbf{v}_h \cdot \nabla_m \\ & + e^4 \mathbf{v}_h \cdot \nabla_s + e^2 (\alpha_w w_1 + \epsilon w^2 \\ & + \dots) \partial_z] (\alpha_w w_1 + \epsilon w^2 + \dots) \\ & + e^2 (2\mathbf{\Omega} \times \mathbf{v})_v - \frac{\bar{\theta}}{1 + \epsilon \bar{\theta}} + \partial_z \bar{\pi} \\ & + \epsilon \bar{\theta} \partial_z \bar{\pi} + e^2 \bar{\theta} \partial_z \bar{\pi} = \epsilon Q_w. \end{aligned} \quad (\text{A15})$$

We use the Taylor series for

$$\frac{1}{1 + \epsilon \bar{\theta}} \approx 1 - \epsilon \bar{\theta} + \dots$$

Including the ansatz for all the variables and separating into different orders of  $\epsilon$  yields:

$$\mathcal{O}(\epsilon^0) : \partial_z \bar{\pi}_0 = \bar{\theta}_0, \quad (\text{A16})$$

$$\mathcal{O}(\epsilon^1) : \partial_z \bar{\pi}_1 = \bar{\theta}_1 - 2\bar{\theta} \bar{\theta}_0, \quad (\text{A17})$$

$$\overline{\mathcal{O}(\epsilon^1)} : \partial_z \bar{\pi}_{1,s} = \bar{\theta}_{1,s} - 2\bar{\theta} \bar{\theta}_0, \quad (\text{A18})$$

$$\mathcal{O}(\epsilon^1)_{\text{res}} : \partial_z \bar{\pi}_{1,m} = \bar{\theta}_{1,m}. \quad (\text{A19})$$

## A.4 Horizontal momentum equation

$$\begin{aligned} & [\epsilon \partial_{t_m} + e^2 \partial_{t_s} + \epsilon \mathbf{v}_h \cdot \nabla_m + e^2 \mathbf{v}_h \cdot \nabla_s \\ & + \epsilon (\alpha_w w_1 + \epsilon w_2 + \dots) \partial_z] \mathbf{v}_h + \epsilon (2\mathbf{\Omega} \times \mathbf{v})_h \end{aligned} \quad (\text{A20})$$

$$+ (1 + \epsilon \bar{\theta} + e^2 \bar{\theta}) \nabla_m \bar{\pi} + \epsilon (1 + \epsilon \bar{\theta} + e^2 \bar{\theta}) \nabla_s \bar{\pi} = Q_v.$$

Including the ansatz for all the variables and  $\mathbf{\Omega} = \mathbf{k}(f_0 + \epsilon \beta y_s)$  and separating into different orders of  $\epsilon$  yields

$$\begin{aligned} \mathcal{O}(\epsilon^1) : & \partial_{t_m} \mathbf{v}_{h,0} + \mathbf{v}_{h,0} \cdot \nabla_m \mathbf{v}_{h,0} + \alpha_w w_1 \partial_z \mathbf{v}_{h,0} \\ & + f_0 \mathbf{k} \times \mathbf{v}_{h,0} + \nabla_m \bar{\pi}_1 + \nabla_s \bar{\pi}_0 = Q_{v,1}, \end{aligned} \quad (\text{A21})$$

$$\begin{aligned} \overline{\mathcal{O}(\epsilon^1)} : & \overline{\mathbf{v}_{0,m} \cdot \nabla_m \mathbf{v}_{0,m}} + \overline{\alpha_w w_1 \partial_z \mathbf{v}_{0,m}} \\ & = \overline{\alpha_w \frac{\mathbf{v}_{0,m}}{\bar{p}} \partial_z (\bar{p} w_1)} \\ & + f_0 \mathbf{k} \times \mathbf{v}_{0,s} + \nabla_s \bar{\pi}_0 = 0, \end{aligned} \quad (\text{A22})$$

$$\begin{aligned} \mathcal{O}(\epsilon^1)_{\text{res}} : & \partial_{t_m} \mathbf{v}_{0,m} + (\mathbf{v}_{0,m} \cdot \nabla_m \mathbf{v}_{0,m})_{\text{res}} \\ & + (\alpha_w w_1 \partial_z \mathbf{v}_{0,m})_{\text{res}} + f_0 \mathbf{k} \times \mathbf{v}_{0,m} + \nabla_m \bar{\pi}_{1,m} \\ & + \mathbf{v}_{0,s} \cdot \nabla_m \mathbf{v}_{0,m} + \alpha_w w_1 \partial_z \mathbf{v}_{0,s} = Q_{v,1}. \end{aligned} \quad (\text{A23})$$

Note that we can rewrite Equation A22 using Equation A2 (continuity equation) as

$$\frac{\alpha_w}{\bar{p}} \partial_z (\overline{\bar{p} w_1 \mathbf{v}_{0,m}}) + f_0 \mathbf{k} \times \mathbf{v}_{0,s} + \nabla_s \bar{\pi}_0 = 0. \quad (\text{A24})$$

For the next order in  $\epsilon$ , we obtain

$$\begin{aligned} \mathcal{O}(\epsilon^2) : & \partial_{t_m} \mathbf{v}_{h,1} + \partial_{t_s} \mathbf{v}_{h,0} + \mathbf{v}_{h,0} \cdot \nabla_m \mathbf{v}_{h,1} \\ & + \mathbf{v}_{h,1} \cdot \nabla_m \mathbf{v}_{h,0} + \mathbf{v}_{h,0} \cdot \nabla_s \mathbf{v}_{h,0} + \alpha_w w_1 \partial_z \mathbf{v}_{h,1} \end{aligned}$$

$$\begin{aligned}
& + w_2 \partial_z \mathbf{v}_{h,0} + f_0 \mathbf{k} \times \mathbf{v}_{h,1} + \beta y_s \mathbf{k} \times \mathbf{v}_{h,0} \\
& + \nabla_m \tilde{\pi}_2 + \bar{\theta} \nabla_m \tilde{\pi}_1 + \nabla_s \tilde{\pi}_1 + \bar{\theta} \nabla_s \tilde{\pi}_0 = Q_{v,2}. \quad (\text{A25})
\end{aligned}$$

$$\begin{aligned}
\overline{\mathcal{O}(\epsilon^2)} & : \partial_t \mathbf{v}_{0,s} + \mathbf{v}_{0,s} \cdot \nabla_s \mathbf{v}_{0,s} \\
& + \underbrace{\overline{\mathbf{v}_{0,m} \cdot \nabla_m \mathbf{v}_{1,m} + \mathbf{v}_{1,m} \cdot \nabla_m \mathbf{v}_{0,m}}}_{\substack{\mathbf{v}_{0,m} (\nabla_s \cdot \mathbf{v}_{0,m} + \frac{1}{p} \partial_z (\bar{p} w_2)) + \frac{\alpha_w}{p} \mathbf{v}_{1,m} \partial_z (\bar{p} w_1) - \alpha_w \mathbf{v}_{0,m} Q_{\theta,2}} \\
& + \overline{\mathbf{v}_{0,m} \cdot \nabla_s \mathbf{v}_{0,m}} \\
& + \overline{\alpha_w w_1 \partial_z \mathbf{v}_{1,m} + w_2 \partial_z \mathbf{v}_{0,m}} \\
& + \overline{f_0 \mathbf{k} \times \mathbf{v}_{1,s} + \beta y_s \mathbf{k} \times \mathbf{v}_{0,s} + \nabla_s \tilde{\pi}_{1,s}} \\
& + \overline{\bar{\theta} \nabla_s \tilde{\pi}_{0,s}} = Q_{v,2,s}. \quad (\text{A26})
\end{aligned}$$

$$\begin{aligned}
\mathcal{O}(\epsilon^2)_{\text{res}} & : \partial_t \mathbf{v}_{1,m} + \partial_t \mathbf{v}_{0,m} \\
& + (\mathbf{v}_{0,m} \cdot \nabla_m \mathbf{v}_{1,m})_{\text{res}} + (\mathbf{v}_{1,m} \cdot \nabla_m \mathbf{v}_{0,m})_{\text{res}} \\
& + (\mathbf{v}_{0,m} \cdot \nabla_s \mathbf{v}_{0,m})_{\text{res}} + \alpha_w (w_1 \partial_z \mathbf{v}_{1,m})_{\text{res}} \\
& + (w_2 \partial_z \mathbf{v}_{0,m})_{\text{res}} + \mathbf{v}_{0,s} \cdot \nabla_m \mathbf{v}_{1,m} + \mathbf{v}_{1,s} \cdot \nabla_m \mathbf{v}_{0,m} \\
& + \mathbf{v}_{0,m} \cdot \nabla_s \mathbf{v}_{0,s} + \mathbf{v}_{0,s} \cdot \nabla_s \mathbf{v}_{0,m} \\
& + \alpha_w w_1 \partial_z \mathbf{v}_{1,s} + w_2 \partial_z \mathbf{v}_{0,s} + f_0 \mathbf{k} \times \mathbf{v}_{1,m} \\
& + \beta y_s \mathbf{k} \times \mathbf{v}_{0,m} + \nabla_m \tilde{\pi}_{2,m} + \bar{\theta} \nabla_m \tilde{\pi}_{1,m} \\
& + \nabla_s \tilde{\pi}_{1,m} = Q_{v,2,m}. \quad (\text{A27})
\end{aligned}$$

We can use Equations A2 and A5 in Equation A26 to rewrite the eddy advection terms.

### A.5 Mesoscale vorticity equation

For each given horizontal momentum equation, we can now compute a corresponding vorticity equation.

We apply  $\mathbf{k} \cdot \nabla_m \times$  to Equation A23 to obtain the mesoscale vorticity equation:

$$\begin{aligned}
\partial_t \zeta_m + \mathbf{k} \cdot \nabla_m \times \underbrace{(\mathbf{v}_{0,m} \cdot \nabla_m \mathbf{v}_{0,m})_{\text{res}}}_{= (\mathbf{v}_{0,m} \cdot \nabla_m \zeta_m)_{\text{res}} + (\zeta_m \nabla_m \cdot \mathbf{v}_{0,m})_{\text{res}}} \\
+ \alpha_w \mathbf{k} \cdot \nabla_m \times (w_1 \partial_z \mathbf{v}_{0,m})_{\text{res}} \\
+ \mathbf{k} \cdot \nabla_m \times (f_0 \mathbf{k} \times \mathbf{v}_{0,m}) \\
+ \underbrace{\mathbf{k} \cdot \nabla_m \times (\nabla_m \tilde{\pi}_{1,m})}_{=0} \\
+ \mathbf{k} \cdot \nabla_m \times (\mathbf{v}_{0,s} \cdot \nabla_m \mathbf{v}_{0,m}) \\
+ \alpha_w \mathbf{k} \cdot \nabla_m \times (w_1 \partial_z \mathbf{v}_{0,s}) = \mathbf{k} \cdot \nabla_m \times Q_{v,1}, \quad (\text{A28})
\end{aligned}$$

where the mesoscale vorticity is defined as  $\zeta_m = \mathbf{k} \cdot \nabla_m \times \mathbf{v}_{0,m}$ . Since  $\nabla_m \cdot (\zeta_m + f_0) \mathbf{v}_{0,m} = 0$ , according to the sub-linear growth criterion, we obtain

$$\begin{aligned}
\partial_t \zeta_m + \nabla_m \cdot ((\zeta_m + f_0) \mathbf{v}_{0,m}) \\
+ \alpha_w (\mathbf{k} \cdot \nabla_m w_1 \times \partial_z \mathbf{v}_{0,m})_{\text{res}} + \alpha_w (w_1 \partial_z \zeta_m)_{\text{res}}
\end{aligned}$$

$$\begin{aligned}
& + \mathbf{v}_{0,s} \cdot \nabla_m \zeta_m + \alpha_w \mathbf{k} \cdot \nabla_m w_1 \times \partial_z \mathbf{v}_{0,s} \\
& = \mathbf{k} \cdot \nabla_m \times Q_{v,1}. \quad (\text{A29})
\end{aligned}$$

### A.6 Synoptic PV equation

We apply  $\mathbf{k} \cdot \nabla_s \times$  to Equation A26 to obtain the vorticity equation for the synoptic scale:

$$\begin{aligned}
\partial_t \zeta_s + \mathbf{v}_{0,s} \cdot \nabla_s \zeta_s + \underbrace{f_0 \nabla_s \cdot \mathbf{v}_{1,s}}_{= -\frac{f_0}{p} \partial_z (\bar{p} w_{3,s})} + \underbrace{\beta y_s \nabla_s \cdot \mathbf{v}_{0,s}}_{=0} \\
+ \beta y_{0,s} \mathbf{k} \cdot \nabla_s \times \left( \overline{\mathbf{v}_{0,m} (\nabla_s \cdot \mathbf{v}_{0,m})} + \overline{\mathbf{v}_{0,m} \frac{1}{p} \partial_z (\bar{p} w_2)} \right) \\
+ \frac{\alpha_w}{p} \mathbf{k} \cdot \nabla_s \times \partial_z (\bar{p} \mathbf{v}_{1,m} w_1) + \mathbf{k} \cdot \nabla_s \times (\overline{\mathbf{v}_{0,m} \cdot \nabla_s \mathbf{v}_{0,m}}) \\
+ \mathbf{k} \cdot \nabla_s \times (\overline{w_2 \partial_z \mathbf{v}_{0,m}}) \\
= \mathbf{k} \cdot \nabla_s \times Q_{v,2,s} + \alpha_w \mathbf{k} \cdot \nabla_s \times (\overline{\mathbf{v}_{0,m} Q_{\theta,2}}). \quad (\text{A30})
\end{aligned}$$

The synoptic-scale vorticity is defined as  $\zeta_s = \mathbf{k} \cdot \nabla_s \times \mathbf{v}_{0,s}$ . We obtain an equation for the potential vorticity by using the thermodynamic equation for  $w_{3,s}$ :

$$w_{3,s} = \frac{1}{\partial_z \bar{\theta}} \left( -\partial_t \tilde{\theta}_0 - \mathbf{v}_{0,s} \cdot \nabla_s \tilde{\theta}_0 - \frac{\alpha_w}{p} \partial_z (\bar{p} w_1 \tilde{\theta}_{1,m}) + \overline{Q_{\theta_4}} \right), \quad (\text{A31})$$

and the potential vorticity

$$q_s = \mathbf{k} \cdot \nabla_s \times \mathbf{v}_{0,s} + \beta y_s + \frac{f_0}{p} \partial_z \left( \frac{\bar{p}}{\partial_z \bar{\theta}} \tilde{\theta}_0 \right) :$$

$$\begin{aligned}
\partial_t q_s + \mathbf{v}_{0,s} \cdot \nabla_s q_s \\
+ \mathbf{k} \cdot \nabla_s \times \underbrace{\left( \overline{\mathbf{v}_{0,m} (\nabla_s \cdot \mathbf{v}_{0,m})} + \overline{\mathbf{v}_{0,m} \cdot \nabla_s \mathbf{v}_{0,m}} \right)}_{\substack{\partial_x \partial_y \overline{v_{0,m} v_{0,m}} - \partial_x \partial_y \overline{u_{0,m} u_{0,m}} + \partial_x \partial_x \overline{u_{0,m} v_{0,m}} - \partial_y \partial_y \overline{u_{0,m} v_{0,m}}} \\
+ \frac{1}{p} \mathbf{k} \cdot \nabla_s \times \partial_z (\bar{p} \mathbf{v}_{0,m} w_2) + \frac{\alpha_w}{p} \mathbf{k} \cdot \nabla_s \times \partial_z (\bar{p} \mathbf{v}_{1,m} w_1)}_{\text{vertical eddy fluxes}} \\
+ \underbrace{\frac{\alpha_w f_0}{p} \partial_z \left( \frac{1}{\partial_z \bar{\theta}} \partial_z (\bar{p} w_1 \tilde{\theta}_{1,m}) \right)}_{\text{vert. eddy temperature flux}} \\
= \mathbf{k} \cdot \nabla_s \times Q_{v,2,s} + \alpha_w \mathbf{k} \cdot \nabla_s \times \overline{\mathbf{v}_{0,m} Q_{\theta,2}} + \frac{f_0}{p} \partial_z \left( \frac{\bar{p}}{\partial_z \bar{\theta}} \overline{Q_{\theta_4}} \right). \quad (\text{A32})
\end{aligned}$$

We can further eliminate the source term  $(\mathbf{k} \cdot \nabla_s \times \mathbf{v}_{0,m}) Q_{\theta,2}$  by using the synoptic-scale rotation of Equations A24 (extended geostrophic balance) and A4 (continuity equation):

$$\frac{1}{\bar{p}} \mathbf{k} \cdot \nabla_s \times \partial_z (\overline{pw_1 \mathbf{v}_{0,m}}) = 0. \quad (\text{A33})$$

With the weak temperature balance for  $w_1$  (Equation 28), it follows that

$$\frac{1}{\bar{p}} \mathbf{k} \cdot \nabla_s \times \partial_z \left( \frac{\bar{p}}{\partial_z \theta} \overline{Q_{\theta,2} \mathbf{v}_{0,m}} \right) = 0. \quad (\text{A34})$$

Hence, it is reasonable to assume  $\mathbf{k} \cdot \nabla_s \times \overline{\mathbf{v}_{0,m} Q_{\theta,2}} = 0$ .

Then, the PV equation reduces to the one given in Equation 35.

### A.7 Divergence equations

Taking the mesoscale, horizontal divergence of Equation A23, we obtain an equation that we can solve for  $\tilde{\pi}_{1,m}$ , if trivial boundary conditions (e.g., periodic, vanishing at distance) are used:

$$\begin{aligned} \nabla_m^2 \tilde{\pi}_{1,m} &= -\alpha_w \partial_{t_m} \nabla_m \cdot \mathbf{v}_{0,m} - \nabla_m \cdot (\mathbf{v}_{0,m} \cdot \nabla_m \mathbf{v}_{0,m})_{\text{res}} \\ &\quad - \alpha_w \nabla_m \cdot (w_1 \partial_z \mathbf{v}_{0,m})_{\text{res}} + f_0 \zeta_{0,m} \\ &\quad - \alpha_w \mathbf{v}_{0,s} \cdot \nabla_m (\nabla_m \cdot \mathbf{v}_{0,m}) \\ &\quad + \alpha_w \nabla_m w_1 \cdot \partial_z \mathbf{v}_{0,s} + \nabla_m \cdot Q_{v,1} \\ &= f(\mathbf{v}_{0,m}, \mathbf{v}_{0,s}, w_1, Q_{v,1}). \end{aligned} \quad (\text{A35})$$

## APPENDIX B. SUBLINEAR GROWTH OF $\mathbf{V}_{1,M}$ AND THE VERTICAL QGPV FLUX CLOSURE

Here we discuss the principal line of thought to be followed in the construction of a self-consistent closure of the vertical flux term VIII in the synoptic PV equation (Equation 35). So far, we have not discussed how to exploit fully the information provided by the first-order perturbation equations in Equations A3, A10, A17, and A26 in determining the  $(t_m, x_m)$  dependences of the first-order quantities  $(\mathbf{v}_{1,m}, w_2, \tilde{\pi}_1, \tilde{\theta}_1)$ . Since the vertical velocities  $w_1, w_2$  are given here by the external heat sources through the WTG

principle (see Equation A10), Equations A3, A17, and A25 constitute a linear inhomogeneous system of equations for the  $(t_m, x_m)$  dependences of the remaining unknowns  $U_1 = (\mathbf{v}_{1,m}, \pi_2, \tilde{\theta}_1)$ , once we know the  $(t_m, x_m)$  dependences of the lower order fields  $U_0 = (\mathbf{v}_{h,0}, w_1, \tilde{\pi}_0, \tilde{\pi}_1, \tilde{\theta}_0)$  and the thermodynamic source term  $Q_{\theta,3}$ . We may write this system formally as

$$\partial_{t_m} U_1 + \mathcal{L}[U_0] U_1 = R_1[U_0]. \quad (\text{B1})$$

Here, our notation  $\mathcal{L}[U_0]$  and  $R_1[U_0]$  is meant to indicate that the linear spatial partial differential operator  $\mathcal{L}$  and the right-hand side  $R_1$  may generally depend upon on  $U_0, \partial_{t_m} U_0, \partial_{t_s} U_0, \nabla_m U_0, \nabla_s U_0$ , and  $\partial_z U_0$ . Note, however, that  $\mathcal{L}[U_0]$  has no explicit dependence upon the synoptic-scale derivatives  $\partial_{t_s} U_0$  and  $\nabla_s U_0$  of the leading-order solution.

Generally, solutions to Equation B1 will be superpositions of some particular solution  $U_1^p$ , which may still violate the initial and boundary conditions for  $U_1$ , and an appropriate “homogeneous solution”  $U_1^h$  of the homogeneous Equation B1 with  $R_1 \equiv 0$ , which accommodates the initial and boundary data. Assuming for now that the homogeneous equation system produces bounded solutions in  $t_m, x_m$ , proper application of the sublinear growth condition requires us to constrain the right-hand side  $R_1[U_0]$  in such a way that  $U_0$  remains sublinear in both fast variables,  $t_m$  and  $x_m$ . These constraints will ultimately reduce to new equations involving the—thus far undetermined—synoptic-scale derivatives  $\partial_{t_s} U_0$  and  $\nabla_s U_0$ , that is, we will obtain the desired synoptic-scale dynamical evolution equation for the leading-order solution. Once these constraints are imposed, the solution procedure also generates the explicit  $(t_m, x_m)$  dependences of  $U_1$ , and hence of  $\mathbf{v}_1, \mathbf{v}_{1,m}$ , and will thus allow us to compute the hitherto unclosed term VIII in Equation 35 in terms of  $U_0$ .

Working out the details of this procedure for specific flows can be arduous, and is therefore left for a future publication.